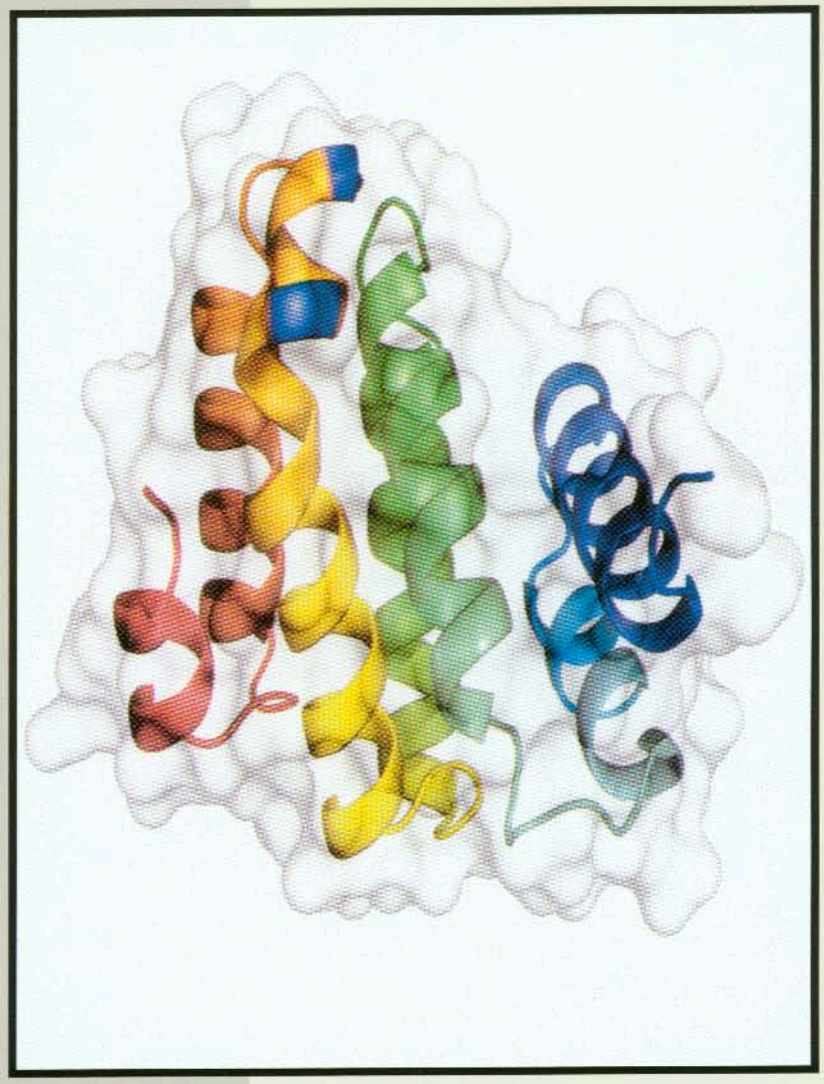

Published Twice Monthly
January 2007, Volume 27, Number 1

AMERICAN
SOCIETY FOR
MICROBIOLOGY

MCB

Molecular and Cellular Biology

MOLECULAR AND CELLULAR BIOLOGY, Jan. 2007, p. 147–156 Vol. 27, No. 1
0270-7306/07/$08.00+0 doi:10.1128/MCB.00867-06

Structural Basis for Inhibition of Translation by the Tumor Suppressor Pdcd4[▽]

Nicole LaRonde-LeBlanc,[1]†* Arti N. Santhanam,[2]† Alyson R. Baker,[2] Alexander Wlodawer,[1] and Nancy H. Colburn[2]

Macromolecular Crystallography Laboratory[1] and Laboratory of Cancer Prevention,[2] Center for Cancer Research, National Cancer Institute, Frederick, Maryland 21702

Received 15 May 2006/Returned for modification 8 August 2006/Accepted 9 October 2006

The tumor suppressor function of Programmed Cell Death 4 (Pdcd4) is achieved through interactions between Pdcd4 and components of the translation initiation complex, namely, the RNA helicase eIF4A and the scaffolding protein eIF4G. These interactions are mediated through two MA3 domains on the Pdcd4 molecule and result in inhibition of protein synthesis. We have solved the high-resolution crystal structure of the C-terminal MA3 (cMA3) domain of Pdcd4 in several crystal forms and demonstrated its similarity to the MA3 domain of eIF4G. As predicted by the structure, the cMA3 domain competes with eIF4Gc for binding to eIF4A and surprisingly is sufficient to inhibit translation initiation. Mutations that abolish eIF4A binding negate both functions of the cMA3. Interestingly mutations in the Akt phosphorylation site influenced neither cMA3 binding to eIF4A nor its ability to inhibit translation initiation. Finally, our structural analysis reveals MA3 domains to be a novel subfamily of VHS domains.

The Programmed Cell Death 4 (*Pdcd4*) gene (also known as *TIS*, *H731*, and *DUG*) was originally described as the apoptosis-associated *MA3* gene in mouse cells (25). Subsequently, Pdcd4 was cloned after differential display analysis of murine JB6 transformation response variants, and its expression was shown to suppress neoplastic transformation (5, 30). Since then there has been considerable interest in the tumor suppressor function of Pdcd4. Pdcd4 protein levels are reduced in human lung-, renal tissue-, and glia-derived tumors (11). Pdcd4 is attenuated with tumor progression in carcinomas of the lung, colon, prostate, and breast. More recently, Pdcd4 has been shown to suppress skin tumorigenesis and tumor progression in transgenic mice (10).

Early insights into the mechanism of tumor suppression by Pdcd4 came from studying the JB6 epidermal model (5). Transformation of JB6 cells requires several events including activation of AP-1- and NF-κB-mediated transcription. Pdcd4 inhibits AP-1-mediated but not NF-κB-mediated transcription (30). This inhibition of AP-1 is indirect and takes place at the level of transcription of the mitogen-activated protein kinase kinase kinase kinase 1/HPK1 kinase upstream of Jun N-terminal kinase in the AP-1 activation pathway (31). Two-hybrid analysis of proteins that interact with Pdcd4 identified two translation initiation factors: eIF4A, an RNA helicase, and eIF4G, a scaffolding protein (8, 29). Pdcd4 interacts with eIF4A and eIF4G via highly conserved MA3 domains, each ~130 amino acids long (28). Pdcd4 must bind to eIF4A to inhibit RNA helicase activity, cap-dependent translation, and AP-1 transactivation. Thus, Pdcd4 is a novel tumor suppressor that inhibits, through its conserved MA3 domains, translation of proteins that are essential for neoplastic transformation as well as tumor invasion.

Dysregulation of protein biosynthesis has been associated with neoplastic transformation and metastasis. In particular, enhanced translation initiation resulting from elevated levels of initiation factors eIF4E, eIF4A, and eIF4G occurs in several human cancers (2, 4, 33). The initiation factors eIF4E, eIF4G, and eIF4A, along with other factors, comprise the eIF4F complex that is crucial for translation initiation and ribosomal assembly on cap-dependent mRNAs. eIF4G binds to eIF4A through a single MA3 domain present in the C-terminal domain of eIF4G (eIF4Gc), as well as through a second motif in the middle domain of eIF4G (eIF4Gm) (Fig. 1). While eIF4A binding to eIF4Gm has been shown to increase helicase activity, eIF4A binding to eIF4Gc is thought to provide a modulatory function (13, 14). Nevertheless, cooperative binding of eIF4A to both eIF4Gm and eIF4Gc domains is important for loading of the 40S ribosome and efficient translation initiation of mRNAs with complex 5′ untranslated region (UTR) structure.

We have previously noted that the MA3 domains of Pdcd4 are similar to the MA3 domain of eIF4Gc and have postulated that one of the MA3 domains interacts with eIF4A through interactions similar to those of the eIF4Gc MA3 domain (32). In order to elucidate the functions of the Pdcd4 MA3 domains, we have solved the crystal structure of the Pdcd4 C-terminal MA3 (cMA3) domain and demonstrated that it effectively competes with the eIF4Gc for binding to eIF4A. In addition, we show that the cMA3 domain alone is sufficient for inhibition of translation. These observations suggest that the cMA3 domain represents a potential candidate for a rationally designed molecule for cancer prevention and intervention.

MATERIALS AND METHODS

Plasmids. The pDEST14-cMA3 expression construct was prepared using Gateway technology to express the C-terminal MA3 domain of mouse Pdcd4

* Corresponding author. Mailing address: Macromolecular Crystallography Laboratory, CCR, National Cancer Institute, Frederick, MD 21702. Phone: (301) 405-0462. Fax: (301) 846-6322. E-mail: nlaronde@umd.edu.

† These authors contributed equally to this work.

▽ Published ahead of print on 23 October 2006.

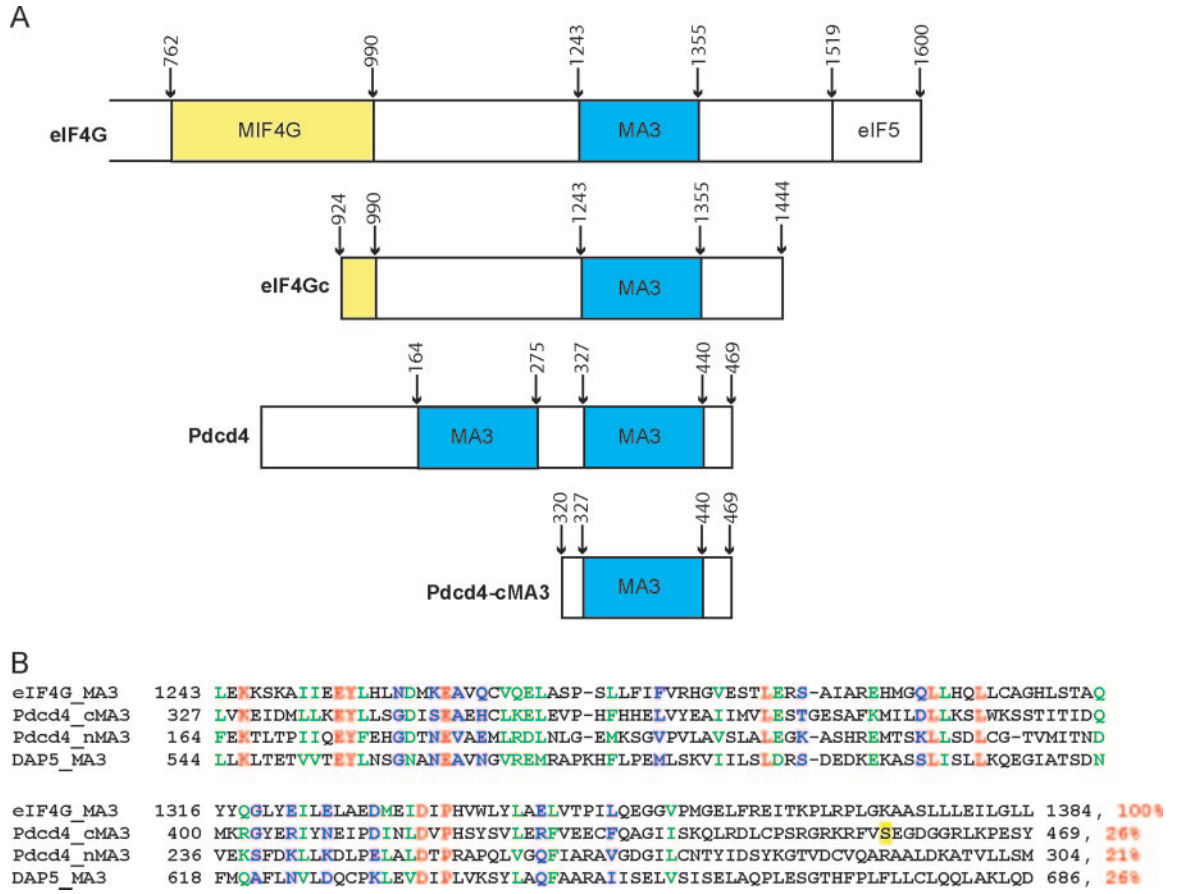

FIG. 1. MA3 domain location and alignments. A. Schematic diagram showing the position of MA3 domains in eIF4G and Pdcd4 and the fragments used in this study. B. Alignment of the MA3 domain of eIF4G, the N-terminal and C-terminal MA3 domains of Pdcd4, and the MA3 domain of DAP5. Residues are colored red for identical, green for highly conserved, and blue for weakly conserved when all four MA3 domains are compared. The residue highlighted in yellow is the Akt phosphorylation site. Percentages in red refer to percent identity compared to the eIF4G MA3 domain.

(residues 320 to 469) with an N-terminal hexahistidine tag connected by a tobacco etch virus protease cleavage site. The mammalian expression vector pCMV-cMA3 was constructed using the Gateway technology by recombination between pENTR-cMA3 and pcDNA-DEST47 (Invitrogen). Plasmids pCMV-BD-Pdcd4, pCMV-BD-eIF4Gc (924–1444), and pCMV-AD-eIF4A used for competition analysis by mammalian two-hybrid assay with the pFR-LUC reporter have been described previously (29). For the translation assays, a stem-loop-structured luciferase vector, pCMV-sl-LUC (29), was transfected with pCMV-cMA3 or its mutants. For immunoprecipitation studies, the plasmid pXpress-eIF4A (32) was transfected along with pHA-eIF4Gc (924–1444) (29), pCMV-Pdcd4, pCMV-cMA3, or its mutants.

Site-directed mutagenesis of His-cMA3. Point mutants of the Pdcd4 cMA3 domain were generated by subjecting the pCMV-cMA3 vector or pCMV-PDCD4(fl) to mutagenesis using the GeneTailor site-directed mutagenesis system (Invitrogen). The following mutagenic oligomers were used (with mutation codons in boldface, 5′→3′): Pdcd4(D414K), forward, GCTATGAGAGAATTTACAATGAAATCCCA**AAG**ATTAATCTGG; reverse, CCAGATTAAT**CTT**TGGGATTTCATTGTAAATTCTCTCATAGC; Pdcd4(D418A), forward, CCCAGACATTAATCTG**GCT**GTCCCACACTCATACTCTG; reverse, CAGAGTATGAGTGTGGGACAGCCAGATTAATGTCTGGG; Pdcd4(S457D), forward, GGGGAAGAAAGCGTTTTGTA**GAT**GAAGGAGATGGAGGCCG; reverse, CGGCCTCCATCTCCTTC**ATC**TACAAAACGCTTTCTTCCCC; Pdcd4(S457A), forward, GGGGAAGAAAGCGTTTTGTA**GCT**GAAGGAGATGGAGGCCG; reverse, CGGCCTCCATCTCCTTC**AGC**TACAAAACGCTTTCTTCCCC.

Protein expression and purification. The His-cMA3 recombinant protein was expressed in *Escherichia coli* (Rosetta DE3-pLysS; Novagen) at 37°C and was present in the soluble fraction. The cells were lysed in a buffer containing 50 mM Tris, pH 8.0, 150 mM NaCl, 0.2% β-mercaptoethanol, 0.2× Bugbuster (Novagen), and 0.1 mg/ml DNase I. The protein was purified by affinity purification on a His-Trap column (GE Healthcare) followed by cleavage of the hexahistidine tag by tobacco etch virus protease and a second pass over the His-Trap column to remove both the tag and the uncleaved molecules. The protein was then further purified by ion-exchange chromatography using a Hi-Trap QHP column (GE Healthcare) and by size-exclusion chromatography using a Superdex 75 column (GE Healthcare). Mass spectrometry of the purified material indicated that the recombinant protein was present in its entirety and was unmodified. Selenomethionine-derivatized protein was produced by expression of the protein overnight at 20°C in minimal medium containing selenomethionine in place of methionine.

Preparation of cell lysates and Western blotting. RT101 cells (4×10^5 cells/100-mm plate) were transiently transfected with 8 μg of wild-type/mutant pCMV-cMA3 vectors or wild-type or mutant pCMV-Pdcd4(fl) vectors. After 4 h, cells were incubated with fresh Eagle's minimal essential medium (EMEM) containing 4% fetal bovine serum (FBS). At 48 h, cells were lysed with 300 μl of nondenaturing lysis buffer (20 mM HEPES-KOH at pH 7.6, 100 mM KCl, 0.5 mM EDTA, 20% glycerol, 0.5% Triton X-100, 50 μg/ml RNase A, 1× protease inhibitor cocktail) for 30 min at 4°C. A 10-μg aliquot of each lysate was separated by 12% sodium dodecyl sulfate-polyacrylamide gel electrophoresis and transferred to a nitrocellulose membrane. The protein-bound membrane was blotted with anti-human PDCD4 antibody.

Protein crystallization and data collection. The initial crystals were obtained by hanging drop vapor diffusion from a reservoir containing either 20% polyethylene glycol (PEG) 1000 and 0.1 M HEPES, pH 7.5, or 20% PEG 3000 and 0.1 M Tris, pH 8.0, at 20°C. Optimized crystals were grown in 20% PEG 1000, 0.1 M HEPES, pH 7.5, and 5% glycerol. Form I crystals belonged to space group $P3_121$

TABLE 1. Data collection and refinement statistics for the cMA3 domain of Pdcd4

Parameter	Selenomethionine SAD[a] form I	Form I	Form II	Form III
Space group	$P3_121$	$P3_121$	$P3_121$	C2
a (Å)	64.45	64.65	61.54	68.25
b (Å)	64.45	64.65	61.54	64.02
c (Å)	170.1	164.7	78.07	38.45
α (°)	90	90	90	90
β (°)	90	90	90	114.15
γ (°)	120	120	120	90
λ (Å)	0.96830	0.97174	1.54	0.97931
Resolution (Å)	30–2.44	30–2.00	30–1.57	30–1.76
R_{sym} (last shell)	0.051 (0.285)	0.069 (0.563)	0.080 (0.501)	0.033 (0.248)
Reflections (no.)	28,519	25,810	23,008	14,183
Redundancy	3.7 (2.6)	4.7 (3.3)	5.1 (4.6)	3.7 (3.3)
Completeness (%)	96.1 (75.1)	98.1 (95.9)	99.6 (95.5)	99.5 (95.6)
R/R_{free} (%)		26.1/29.7	16.0/19.4	19.5/24.9
Mean B factor (Å^2)		51.4	15.3	32.1
Residues (no.)		127/127	129	126
Waters (no.)		50	189	116
RMS deviation				
Length (Å)		0.018	0.022	0.021
Angle (°)		1.48	1.78	1.79

[a] SAD, single-wavelength anomalous dispersion.

with two molecules per asymmetric unit and diffracted to a resolution of 2.4 Å. Subsequent improvement in cryoprotection resulted in improved diffraction to 2.0 Å. Cryoprotection was performed by stepwise transfer into well solution containing 10% ethylene glycol over a 5-min period. The second crystal form (form II) was obtained in 0.17 M ammonium sulfate, 0.085 M sodium acetate, pH 4.6, 25.5% (wt/vol) PEG 2000 monomethyl ether, 15% (vol/vol) glycerol. This was sufficient for cryoprotection. The third crystal form (form III) was obtained in 10% (wt/vol) PEG 3000, 100 mM phosphate-citrate, pH 4.2, 200 mM NaCl. Fifteen percent (wt/vol) glycerol was added to this solution for cryoprotection.

Structure determination. Single-wavelength anomalous dispersion data were collected at the peak wavelength at the selenium K edge using selenomethionine-derivatized protein crystals at the Southeast Regional Collaborative Access Team (Advanced Photon Source, Argonne National Laboratory, Argonne, IL). All eight selenium sites were found using SOLVE (26), whereas RESOLVE was used to perform density modification and build some of the model into the resulting electron density map. Several rounds of model building and refinement were performed using Xtalview (18) or Coot (7) for model building and Refmac5 (21) for refinement. Data and refinement statistics are provided in Table 1. Subsequent structures were determined by molecular replacement using molecule A of the structure determined by selenomethionine phasing.

Cap-dependent translation assays. RT101 cells (1.5×10^4) were seeded in 24-well plates in EMEM with 4% FBS and transfected with 0 to 300 ng of wild-type/mutant pCMV-cMA3 vector or 0 to 200 ng of wild-type or mutant pCMV-Pdcd4(fl) vectors, 25 ng of stem-loop-structured luciferase vector, and 5 ng of thymidine kinase-*Renilla* luciferase gene in Fugene (Roche). Total DNA was equalized using pDEST47 or pCMV3.1+ vector control. After 4 h, cells were incubated with fresh EMEM containing 4% FBS. At 48 h, cells were lysed in 100 μl of 1× passive lysis buffer (Promega). Then 25-μl aliquots of the lysates were analyzed for luminescent signal with a microtiter plate luminometer (Dynex Technologies). Values (average light units) were expressed as the means ± standard deviations. Experiments were repeated three times in sextuplicate, and representative data are shown as percentages of control.

Mammalian two-hybrid competition assay. The mammalian two-hybrid assay was done as previously described (28). Briefly, RT101 cells (1.5×10^4) were seeded in 24-well plates in EMEM with 4% FBS. After 16 h, cells were transfected with 50 ng of pCMV-BD-eIF4G(497–974), 400 ng of pCMV-AD-eIF4A, and 25 ng of pFR-LUC Gal4-luciferase reporter gene (Stratagene), along with increasing concentrations of pCMV-cMA3 (or its mutants) or wild-type or mutant pCMV-Pdcd4(fl) vectors in Fugene (Roche) for 4 h. Total DNA was kept equal using vector control. Cells were then incubated with fresh EMEM containing 4% FBS. At 48 h, cells were lysed in 100 μl of 1× passive lysis buffer (Promega). Then 25-μl aliquots of the lysates were analyzed for luminescent signal with a microtiter plate luminometer (Dynex Technologies). Values (average light units) were expressed as the means ± standard deviations. Experiments were repeated two times in sextuplicate, and representative data are shown as percentages of control.

Protein structure accession numbers. The coordinates and structure factors for the three crystal forms have been deposited in the Protein Data Bank (PDB) with accession codes 2IOL, 2ION, and 2IOS. Coordinates for crystal form II refined to 615 Å have been deposited with code 2NSZ.

RESULTS

Crystallization and structure determination. A fragment of mouse Pdcd4 identified by sequence alignment to contain the C-terminal MA3 domain (cMA3; residues 320 to 469 [end]) was expressed in *E. coli* and purified for crystallization. Form I crystals that were obtained initially belonged to space group $P3_121$ with the cell dimensions $a = b = 64.45$ Å, $c = 170.1$ Å, and contained two monomers per asymmetric unit. The structure was solved by single-wavelength anomalous dispersion for a selenomethionine derivative; phases were obtained to produce an electron density map at 2.44-Å resolution. An initial model was built using this map and refined to 2.0 Å using a second data set from a similar crystal. Although that model was in excellent agreement with the electron density for molecule A, the density for molecule B was not satisfactory. Several indications, such as the location of the selenium atoms based on anomalous signal, supported the placement of both molecules, yet the refinement did not proceed as expected, resulting in an R factor and R_{free} of 0.26 and 0.30, respectively. Subsequently, we obtained a second, closely related, crystal form (form II) that did not exhibit such problems. These crystals also belong to space group $P3_121$ with the cell dimensions $a = b = 61.42$, $c = 78.04$ Å, with one molecule per asymmetric unit. Data from one crystal extending to 1.57-Å resolution were used for the final refinement steps. The model was refined to an R factor of 0.16 and R_{free} of 0.19, with good stereochemistry (Table 1). That model contains 129 out of 150 residues in each

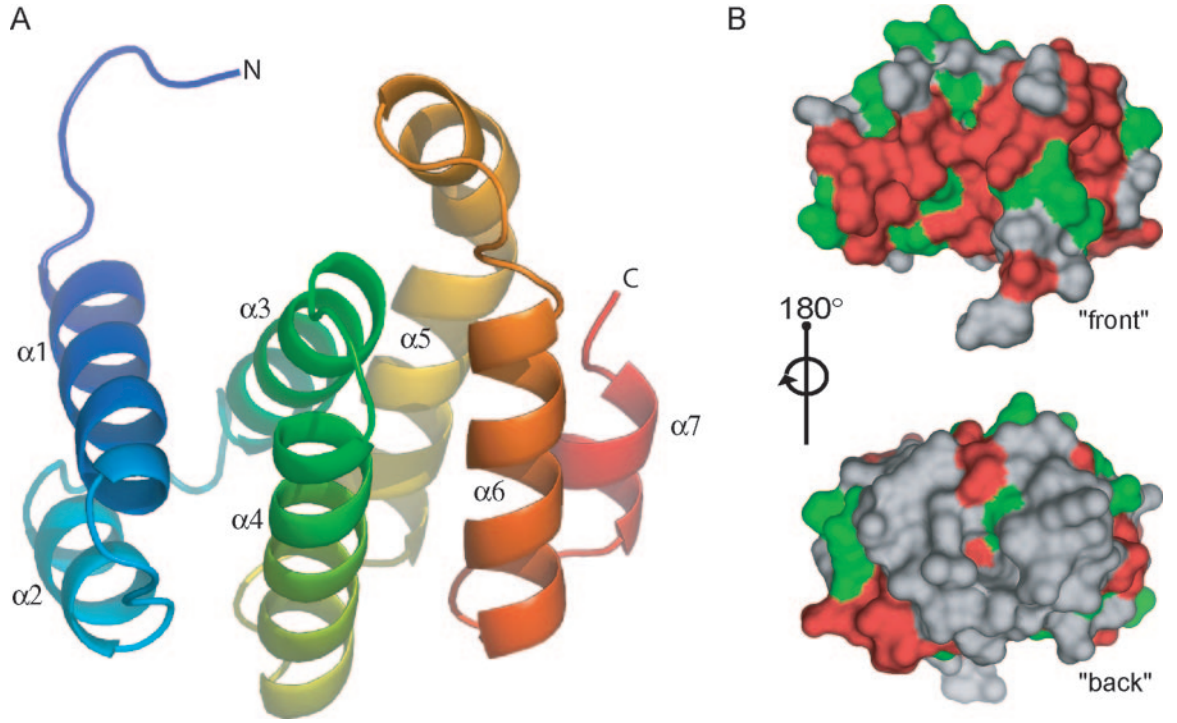

FIG. 2. Crystal structure of the C-terminal MA3 domain of Pdcd4. A. Ribbon diagram showing the seven-α-helix structure of the MA3 domain. B. Surface representation of the MA3 domain of Pdcd4 colored by conservation of residues among Pdcd4 proteins from various species (red, identical; green, highly conserved). All figures of the structure were made using Pymol (http://www.pymol.org).

molecule, from residue 322 to residue 450. The first two residues and the last 20 residues of the recombinant protein were not built due to the lack of electron density in those regions. A third crystal form, this one obtained in space group C2, was also refined, confirming the models built in the first two forms. The models derived from the three crystal forms are very similar (root mean square [RMS] deviation between the Cα coordinates of molecule A of form I and the sole molecule of form II is 0.63 Å, and that between form II and form III is 0.49 Å). The coordinates derived from form II crystals are used in all discussions below, since they correspond to the highest-resolution data.

Overall structure of the cMA3 domain of Pdcd4. A ribbon diagram showing the architecture of the MA3 domain is shown in Fig. 2A. The domain consists of seven α-helices, which pack into a globular form. Analogous to HEAT domains, the packing arrangement consists of repeating pairs of antiparallel helices packed one upon the other such that a superhelical axis is generated perpendicular to the α-helical axes. The second pair, α3 and α4, is rotated relative to the first pair, α1 and α2, by ~60°. The third pair, α5 and α6, is rotated relative to the second pair by ~40°. The final α-helix, α7, packs between the latter pair of α-helices to cap off the domain and is the last-ordered portion of Pdcd4. The remaining 20 residues on the C terminus, which includes a recently characterized Akt phosphorylation site at S457 (23), are not seen in the electron density. Hydrophobic interactions between conserved residues stabilize the interaction between the pairs of helices and between adjacent repeats.

Most of the residues conserved between all known MA3 domains appear to map at the interfaces between helices and helical repeats. These residues are involved in interactions that stabilize the three-dimensional structure of the protein. Analysis of the position of the residues conserved between the cMA3 domains of Pdcd4 in humans and other species indicates that these residues appear to map primarily to one surface of the molecule (Fig. 2B). We will refer to this surface as the "front" and the opposite surface as the "back."

The MA3 domains of Pdcd4 and eIF4G have similar structures. A crystal structure for the C-terminal fragment of eIF4G is available in the Protein Data Bank (PDB; accession code 1ug3) (3). This set of coordinates includes two crystallographically independent molecules, each consisting of residues 1234 to 1566 of eIF4G. The segment 1234 to 1427 includes the putative MA3 domain of eIF4G (eIF4Gc), whereas the segment 1438 to 1566 has been annotated as an "eIF5-like domain" (Fig. 1A). A comparison of the MA3 domains of Pdcd4 and eIF4G has revealed the structural features that are characteristic for the MA3 domains (Fig. 3). The two structures, Pdcd4 residues 323 to 448 and eIF4G residues 1237 to 1367, align with RMS deviations of 1.76 Å for 115 Cα pairs, and the Z score reported by the program DALI (9) is a very significant 16.4 (Fig. 3A and B). The length of the helices and loops in between them appears to be remarkably conserved between the two proteins. Also, the angles between the pairs of helices, which would have an effect on the shape of the molecule, all appear to be conserved. The two proteins exhibit significant sequence homology (25% of residues are identical, and 30% strongly similar; Fig. 1B). Residues that are identical between the two molecules map primarily to the front surface of the

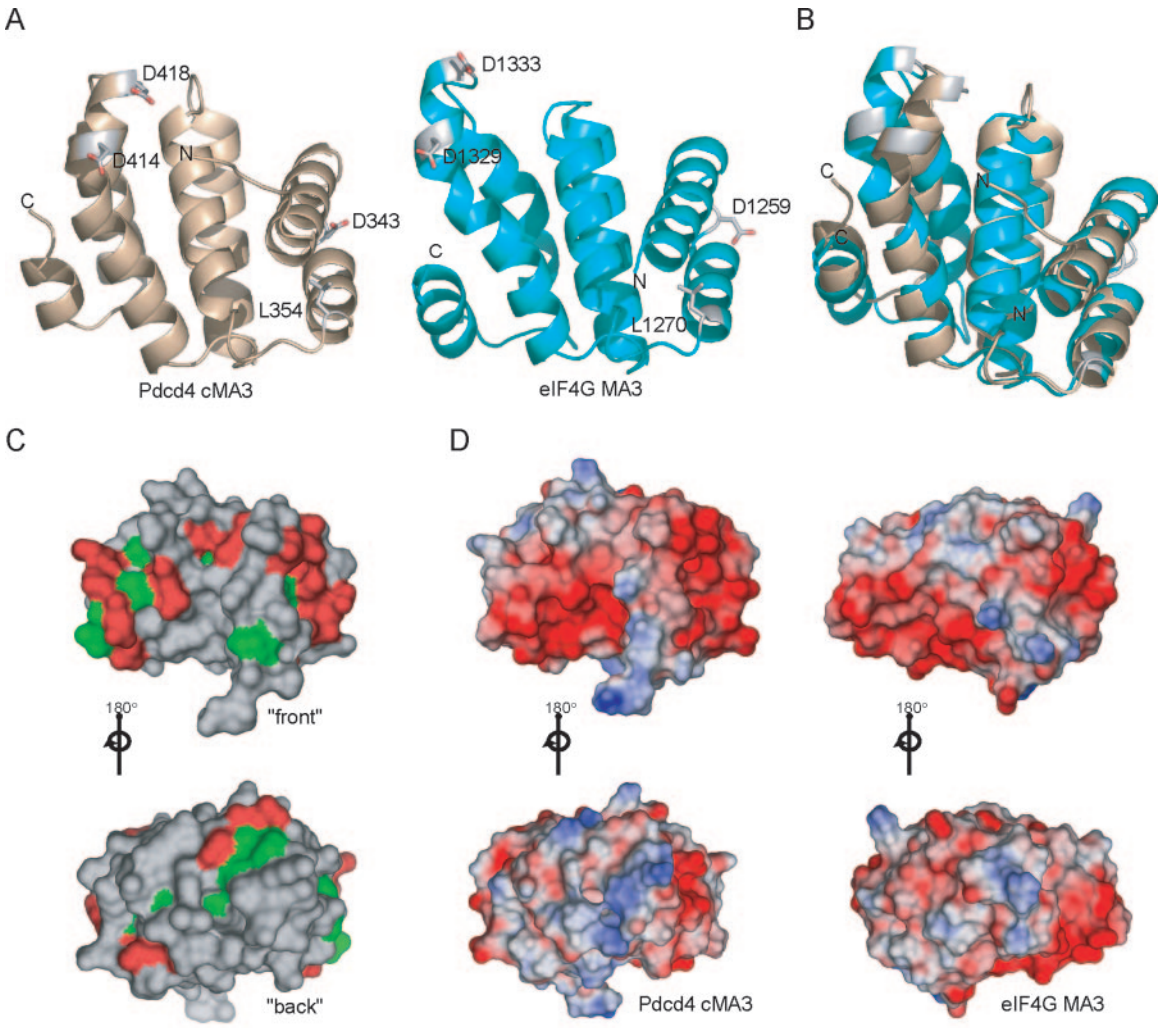

FIG. 3. The MA3 domains of Pdcd4 and eIF4G have similar structures. A. Ribbon representation of the MA3 domains of Pdcd4 (wheat) and eIF4G (cyan; PDB code 1ug3) showing the locations of residues that influence interaction with eIF4A. B. Alignment of the MA3 domains of Pdcd4 and eIF4G. C. Surface representation of the cMA3 domain of Pdcd4 colored by conservation of residues between Pdcd4 and eIF4G (red, identical; green, highly conserved). D. Electrostatic surface representation of the MA3 domains of Pdcd4 and eIF4G (red to blue = -10 κBT to 10 κBT). Electrostatic calculations were performed using APBS (1).

molecule (Fig. 3B). The curvature of the end of the α5 helix is conserved in the MA3 domain but is positioned slightly differently between the eIF4Gc domain and the Pdcd4 cMA3. An analysis of the temperature factors in this region for the Pdcd4 and the eIF4Gc molecule reveals higher-than-average values for both, suggesting that this part of each molecule may be mobile. In addition, comparison of the front surface of the eIF4G MA3 domain and of that of the cMA3 domain of Pdcd4 shows remarkably similar charge distribution (Fig. 3C).

Similarity of the MA3 domain of Pdcd4 and its structural homologs: a novel group of VHS domains. In addition to the similarity of the MA3 domain of Pdcd4 to the eIF4Gc domain, a search with the program DALI (9) identified a number of other protein domains with significant structure homology. The highest scores (9.9 and 9.7) were for the MIF4G domains of human CBP80 (17) (PDB code 1h6k) and of an analogous domain found in the nonsense-mediated mRNA decay factor UPF2 (12) (PDB code 1uw4). The RMS deviations of the Cα coordinates were 2.4 and 3.0 Å for 107 and 114 pairs, respectively (Fig. 4A shows an alignment with the MIF4G domain of eIF4G). Surprisingly, the next highest score was for the C-terminal domain of eIF4G (PDB code 1ug3, residues 1438 to 1566), annotated as an "eIF5-like domain" (24), with RMSs of 2.5 Å for 107 Cα pairs (Fig. 4B). An agreement with the middle domain of eIF4G (16) (PDB code 1hu3), the prototype of MIF4G domains, was marginally lower (Z score, 9.0; RMS deviation, 3.1 Å for 107 Cα pairs [Fig. 4A]). All MIF4G domains consist of 10 helices, the first seven of which align with the MA3 helices. On the other hand, the length of an eIF5-like domain is almost identical to that of the MA3 domain.

The MA3 domain also exhibits significant structural (but not sequence) similarity to VHS domains, found so far only on the amino termini of diverse proteins involved in vesicular trafficking, cytokine-mediated signal transduction, protein targeting, etc. (15). VHS domains contain ~150 residues arranged into eight helices. Helices 1 to 4 create two antiparallel helical

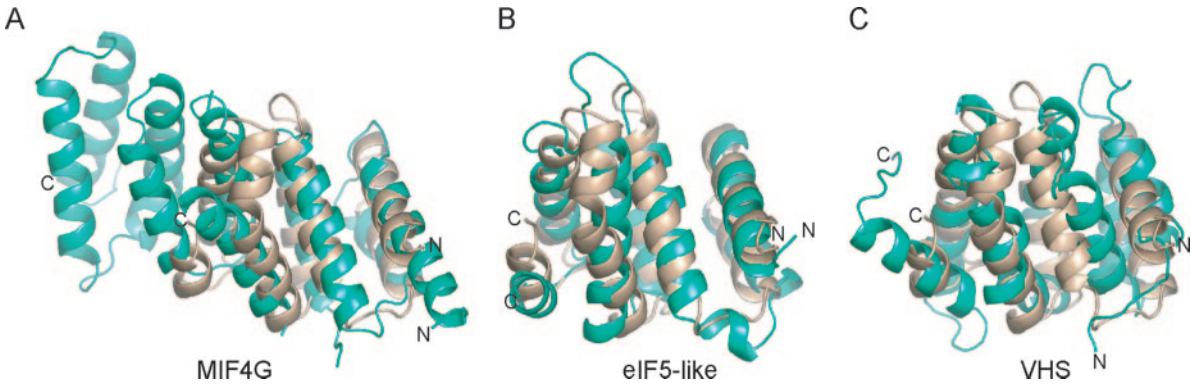

FIG. 4. Comparison of the MA3 domain to its structural homologs. Shown are structural alignments of the cMA3 domain of Pdcd4 (wheat) on the MIF4G domain of eIF4G (green; PDB code 1hu3) (A), the eIF5-like domain of eIF4G (green; PDB code 1ug3) (B), and the VHS domain of Tom1 (PDB code 1elk) (C).

hairpins, helix 5 is perpendicular to the other ones, and helices 6 to 8 are again roughly parallel (or antiparallel) to one another. This arrangement is very similar to the arrangement found in the MA3 domain, with the exception that helix 5 of a typical VHS domain is replaced by an irregular helical turn in MA3. The VHS domain of human Tom1 (19) (PDB code 1elk) can be superimposed on the MA3 domain with an RMS of 3.2 Å for 103 Cα pairs (DALI Z score, 6.9; Fig. 4C), whereas an analogous domain of human signal transducing adaptor molecule 2 (PDB code 1x5b, not published) superimposes with an RMS of 3.4 Å for 111 Cα pairs, when the first of the 20 nuclear magnetic resonance (NMR)-derived models is used for the comparisons. The overall similarity of the length and fold of the MA3 domains of both Pdcd4 and eIF4G to VHS domains suggests that MA3 domains might be described as a novel group of VHS domains.

Functional conservation between the MA3 domains of Pdcd4 and eIF4G. Yang et al. have shown that full-length Pdcd4 competes with eIF4Gc for binding to eIF4A (28). Because the Pdcd4 protein contains two MA3 domains while eIF4Gc contains only one, we hypothesized that at least one of the two MA3 domains of Pdcd4 must closely mimic that of eIF4Gc. Based on sequence alignments (Fig. 1B), we have determined that of the two MA3 domains of Pdcd4, the cMA3 domain of Pdcd4 is more similar to the MA3 domain of eIF4Gc and is the likely candidate for direct competition with eIF4Gc. This distinction is also supported by sequence alignments between the cMA3 and nMA3 sequences that reveal the presence of residues within the nMA3 domain that are likely to produce a structure different from the cMA3 domain. One example is the presence of a proline residue (Pro200) in the middle of what would correspond to the α3 helix in the nMA3 domain (Fig. 2). Both the cMA3 domain of Pdcd4 and the MA3 domain of eIF4G have a valine in this position. The presence of this proline in the nMA3 would likely disrupt or bend the α3 helix and consequently change interactions that position helix α5 (Fig. 2). This Val/Pro change is likely to make the nMA3 less structurally similar than the cMA3 domain to the eIF4G.

Four residues were identified which result in loss of binding either between the MA3 domain of Pdcd4 and eIF4A or between the MA3 domain of eIF4Gc and eIF4A (28). The locations of those residues are shown in Fig. 3A. All four of these residues are present on the front surface of the molecule and are therefore accessible to protein-protein interaction. Mutation of two of the four residues, Asp414 and Asp418, located in the bent portion of α5, resulted in the complete loss of eIF4A binding activity (28). Mutation of the analogous residues in eIF4Gc, Asp1329 and Asp1333, produced a similar inactivating effect on binding to eIF4A (28). Death-associated protein 5 (DAP5), which contains a Lys in the Asp414 position, is incapable of binding eIF4A.

Pdcd4 cMA3 domain efficiently competes with eIF4Gc for binding to eIF4A. During translation initiation, the interaction of eIF4A with the scaffolding protein eIF4G is essential for efficient translation of structured mRNA. It has been shown previously that Pdcd4 inhibits translation initiation at least in part by competing with eIF4G for binding to eIF4A (28). Considering the remarkable similarity in the structures of the cMA3 domains in Pdcd4 and eIF4Gc discovered in the course of this study, we were intrigued by the possibility that cMA3 alone might compete with the eIF4G C-terminal domain (eIF4Gc) for binding to eIF4A. As shown in Fig. 5A, increasing concentrations of His-cMA3 produced a dose-dependent decrease in the interaction between eIF4A fused to a Gal4 activation domain and eIF4Gc fused to a Gal4 DNA binding domain in a mammalian two-hybrid assay. The resultant decrease in eIF4A-eIF4Gc interaction due to cMA3 expression (~65%) was comparable to that observed with expression of full-length Pdcd4 (~70%). As expected, when constructs of cMA3 or full-length Pdcd4 containing mutations in the residues important for eIF4A binding (Asp414 and Asp418, Fig. 5A and C) were used in the two-hybrid assay, no disruption of the interaction between eIF4A and eIF4Gc was detected. Moreover, these effects were not due to a decrease in the steady-state expression of the mutant proteins in comparison to the wild type (Fig. 5B and D). Thus, the cMA3 domain alone can efficiently compete with eIF4Gc for binding to eIF4A.

A recent study has implicated the Akt signaling pathway in the regulation of Pdcd4 localization and certain functions (23). Although the Akt-responsive Ser457 residue is present in the Pdcd4 fragment used for crystallization, the lack of electron density for this region excludes Ser457 from the final crystal structure (Fig. 1B and Fig. 2A) and demonstrates the inherent

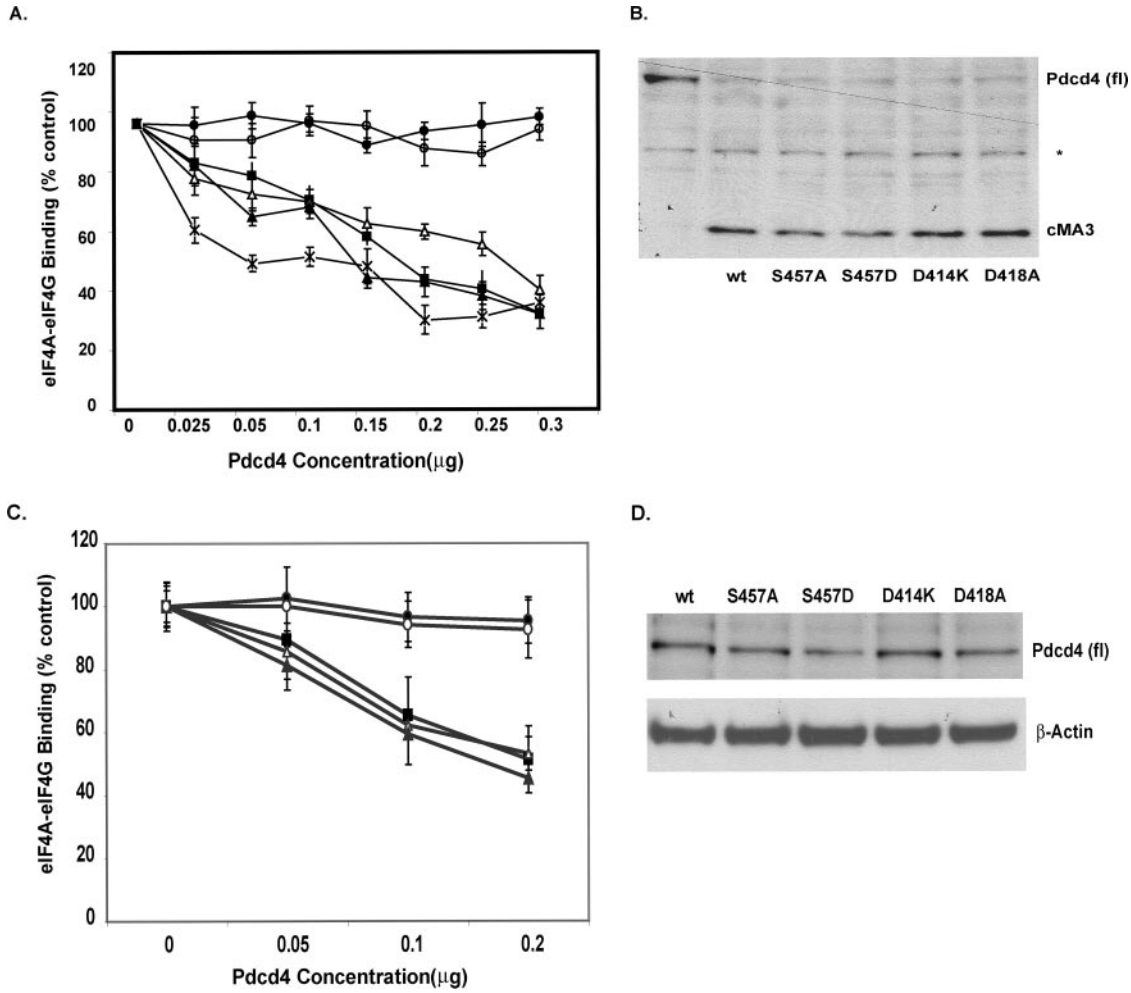

FIG. 5. Pdcd4 cMA3 competes with eIF4Gc for eIF4A binding. (A and C) Increasing amounts (0 to 300 ng) of pCMV-cMA3 (×), mutants (pCMV-cMA3^{D418A} [○], pCMV-cMA3^{S457A} [▲], pCMV-cMA3^{S457D} [△], pCMV-cMA3^{D414K} [●]), or pCMV-Pdcd4(fl) (■) (A) or 0 to 200 ng of pCMV-Pdcd4(fl) (■) or mutants (pCMV-Pdcd4^{D418A} [○], pCMV-Pdcd4^{S457A} [△], pCMV-Pdcd4^{S457D} [▲], or pCMV-Pdcd4^{D414K} [●]) (C) was transiently transfected with pCMV-AD-eIF4A (400 ng), pCMV-BD-eIF4Gc (50 ng), and Gal4-luciferase reporter DNA (25 ng) into JB6 RT101 cells. After 48 h, cells were lysed and the luciferase activity was measured. The luciferase activity from 0 ng of pCMV-cMA3 or mutants was designated as 100%. These experiments were repeated three times with six independent transfections, and representative data are shown. The results are expressed as means ± the standard deviations. At equal concentrations (μg) of plasmids, 1 M equivalent of cMA3 in Pdcd4 (full length) equals 0.8 M equivalent of cMA3 (pCMV-cMA3). (B) Pdcd4 cMA3 mutant expression is comparable to that of wild-type and full-length protein by Western blotting performed on whole-cell lysates from RT101 cells and detected with anti-human PDCD4 antibody. The asterisk shows a nonspecific band. (D) Expression of Pdcd4(fl) and that of mutants were comparable by Western blot detection with anti-human PDCD4 antibody. wt, wild type.

flexibility of this part of the molecule. This flexibility is consistent with the availability of this part of the protein for phosphorylation. In order to decipher the role, if any, of Akt-dependent phosphorylation in the eIF4A binding function of the Pdcd4 cMA3 domain, we engineered mutations at the Ser457 residue that either mimic constitutive phosphorylation (Ser457Asp) or prevent phosphorylation (Ser457Ala). Figure 5A shows that both mutant constructs produced a decrease in interaction between eIF4A and eIF4Gc, similar to that observed with wild-type cMA3 (~60 to 70%). Similar results were obtained by mutations (S457A and S457D) in full-length Pdcd4 (Fig. 5C). This decrease was not due to an increase in steady-state expression of either of the mutant proteins in comparison to the respective wild type (Fig. 5B and 5D). This result suggests that the S457 residue may not be essential for binding interactions between the Pdcd4 cMA3 domain and eIF4A and for the resulting competition with eIF4Gc.

The Pdcd4 cMA3 domain alone is sufficient to inhibit cap-dependent translation. Pdcd4 inhibits translation initiation of cap-dependent mRNAs, in particular mRNAs that possess a highly structured 5′ UTR, by its interaction with the initiation factor eIF4A. Although the analysis of deletion mutants suggested that Pdcd4 needed two MA3 domains to bind to eIF4A and inhibit translation (27), the similarity of crystal structures (Fig. 3A) and the relatively efficient competition with eIF4Gc for binding to eIF4A compared with full-length Pdcd4 (Fig. 5) suggested that cMA3 alone might be an efficient inhibitor of translation. We therefore studied the effect of cMA3 alone on

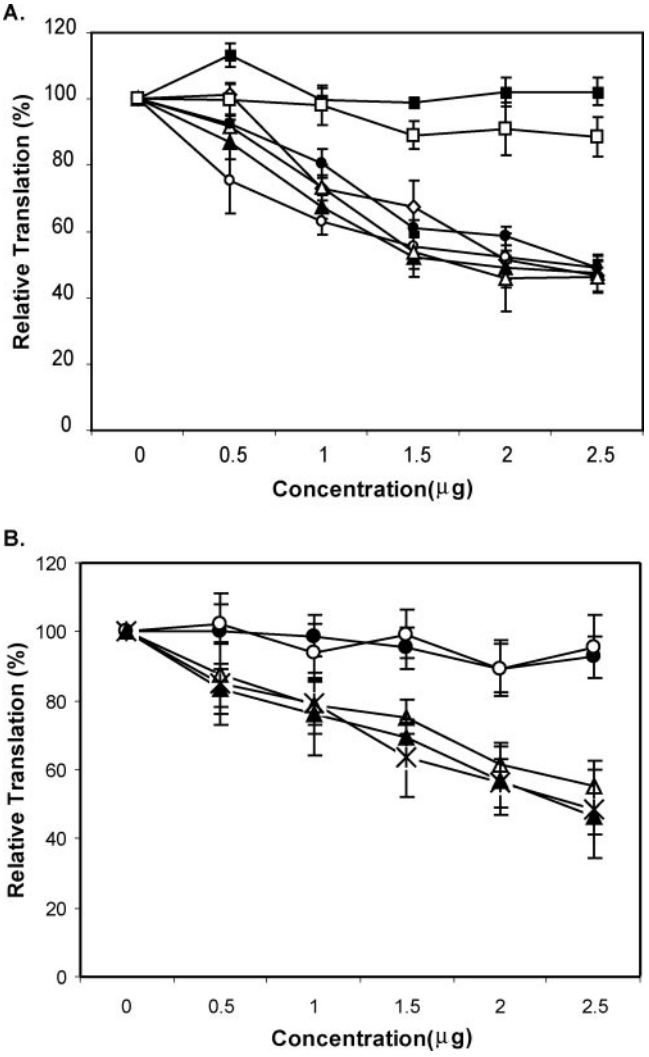

FIG. 6. Pdcd4 cMA3 alone is sufficient to inhibit eIF4F-dependent translation initiation. Increasing amounts (0 to 2.5 μg) of plasmids pCMV-Pdcd4cMA3 (◇), pCMVcMA3^{D418A} (■), pCMVcMA3^{D414K} (□), pCMVcMA3^{S457A} (△), pCMVcMA3^{S457D} (▲), pCMV-Pdcd4(fl) (○), and pCMV-eIF4Gc (●) (A) or pCMV-Pdcd4(fl) (×) or mutants (pCMV-Pdcd4^{D418A} [●], pCMV-Pdcd4^{S457A} [△], pCMV-Pdcd4^{S457D} [▲], and pCMV-Pdcd4^{D414K} [○]) (B) were transiently transfected with pCMV-SL-LUC (0.2 μg) into JB6 RT101 cells. The total DNA was maintained at 2.2 μg by adding appropriate vector DNA. After 48 h, cells were lysed and the luciferase activity was measured. The luciferase activity from the cells with 0 μg of pCMV-Pdcd4 (or mutants) or pCMV-eIF4Gc was designated as 100%. These experiments were repeated three times with six independent transfections, and representative data are shown. The results are expressed as means ± standard deviations. At equal concentrations (μg) of plasmids, 1 M equivalent of cMA3 in Pdcd4 (full length) equals 0.8 M equivalent of cMA3 (pCMV-cMA3).

translation of a structured mRNA in vivo. Interestingly, cMA3 expression alone efficiently inhibited (by ~54%) translation of a stem-loop luciferase reporter mRNA (Fig. 6). This inhibition was dose dependent, and the percent inhibition was comparable to that of full-length Pdcd4 (51%). In addition, cMA3 mutated in residues previously shown to be important for efficient binding to eIF4A (Asp414 [data not shown] and Asp418 [Fig. 6]) did not inhibit translation. As expected, wild-type cMA3 expression produced minimal inhibition of a non-stem-loop mRNA control, whereas the cMA3 (Asp414Lys) and cMA3 (Asp418Ala) mutants were inactive (data not shown). Thus, the cMA3 domain alone appears to be sufficient for specific and efficient inhibition of cap-dependent translation. Because translation inhibition by Pdcd4 may depend not only on competition with eIF4Gc but also on disruption of other interactions important to translation initiation, we asked whether translation would be inhibited by the cMA3 mutated in the Akt site. As shown in Fig. 6A, mutation of Ser457 to Asp or Ala resulted in an efficiency of translation inhibition (~53%) similar to wild-type efficiency (~54%), suggesting that phosphorylation at Ser457 does not regulate the translation inhibition function of the cMA3 domain. Consistent with the binding competition studies, mutations at the Akt site did not affect efficiency of translation inhibition in full-length Pdcd4 either (Fig. 6B). Taken together, these results establish that Pdcd4-cMA3 inhibits translation of 5′-UTR-structured mRNA with an efficiency similar to that of full-length Pdcd4.

DISCUSSION

Previous studies have shown that the full-length Pdcd4, as well as a fragment of Pdcd4 containing the two MA3 domains alone, was capable of inhibiting eIF4A translation initiation activity and protein synthesis by binding to eIF4A. This fragment was capable of competing with the C-terminal domain of eIF4G (eIF4Gc) for binding to eIF4A (28). The study of the cMA3 domain of Pdcd4, presented here, demonstrates how this domain alone mimics the structure and functional binding activity of eIF4Gc, leading to inhibition of translation activation activity of eIF4A.

The crystal structure of the cMA3 domain of tumor suppressor Pdcd4 and comparison with the structure of the MA3 domain of eIF4G have allowed us to characterize the structural features of the MA3 domain. First identified in Pdcd4 (a protein also known as MA3), these domains have also been found in DAP5 and nucleolar protein with MIF4G domain. Our structural analysis indicates that this domain displays significant structural homology to VHS domains and may be considered a subgroup of that family, as evidenced by the conservation of the number of pairs of repeated antiparallel helices and the angle of rotation between subsequent repeats. However, the MA3 domains of Pdcd4 and eIF4A are distinguished by the presence of an unusual turn at the end of helix 5. Interestingly, it is this helix that contains the residues shown to be important for the function of Pdcd4 and eIF4G in binding to eIF4A. Thus, we believe this helix to be an important eIF4A binding motif that distinguishes MA3 domains. While the manuscript was in preparation, an NMR secondary structure assignment was reported for the cMA3 domain of Pdcd4, and it agrees with our crystal structure data (27).

Of the two MA3 domains found in Pdcd4, the cMA3 domain is more similar to the MA3 domain of eIF4G by sequence comparison. A comparison of the structures of the MA3 domains of eIF4Gc and Pcdc4 (cMA3) demonstrates a remarkable similarity between the structures as well. We also observed similarity in the positioning of conserved residues on one surface of the domains and in their electrostatic charge

distribution properties. In particular, the residues Asp414 and Asp418, which are required for eIF4A binding in Pdcd4, are strictly conserved in eIF4G. In the N-terminal MA3 domain of Pdcd4, a glutamate residue replaces Asp414. In addition, Asp414 is replaced by a lysine residue in the MA3 domain of DAP5, which does not bind eIF4A (28). These features suggested to us that the cMA3 domain of Pdcd4 may mimic the binding of eIF4Gc to eIF4A.

As predicted by this hypothesis, the Pdcd4 cMA3 domain alone functioned as an effective competitive inhibitor of the eIF4Gc MA3 domain. Interestingly, given the molar activity similar to that of Pdcd4 (0.8:1.0) and assuming similar protein stability, it appears that the cMA3 domain has affinity similar to, if not higher than, that of the eIF4Gc domain for eIF4A binding. Consistent with the idea that a molecule that competes for the eIF4Gc binding site on eIF4A may inhibit the function of eIF4A, the eIF4Gc domain was also shown to be sufficient to inhibit translation in vitro (20). Although the mechanism of such inhibition is not clear, the eIF4A binding function of the cMA3 domain suggests that it may be through the disruption of the ideal stoichiometry of an active eIF4F complex. In this study, we show that eIF4Gc alone can inhibit stem-loop translation in vivo, and a similar result was seen for the Pdcd4 cMA3 domain. The relative importance of Pdcd4's competition for C-terminal function of eIF4G and its binding to the middle domain of eIF4G in translation inhibition has not been previously elucidated. The observation of similar efficiency for translation inhibition by cMA3, full-length Pdcd4, and eIF4Gc suggests that the competition with eIF4Gc for binding to eIF4A may play a major role in the mechanism of translation inhibition by Pdcd4.

We do not fully understand the function of the N-terminal MA3 domain in Pdcd4. It is expected to be structurally similar to the cMA3 domain structure presented here. However, attempts to build a three-dimensional homology model of the nMA3 domain structure based on the cMA3 domain structure were unreliable due to differences in residues that would likely result in differences in secondary structure and positioning of the helices relative to each other. Given the structural homology between the MA3 domain and the MIF4G domain, it is possible that Pdcd4 nMA3 might mimic the function of the MIF4G domain of eIF4G (eIF4Gm). A model built based on NMR interaction mapping data suggested that the MIF4G domain interacts with eIF4A and holds it in a closed and active conformation (22). Although this may not be the case with Pdcd4, which functions to inhibit the eIF4A function, the nMA3 domain of Pdcd4 may compete with the eIF4G MIF4G domain for eIF4A binding. Another possibility is that the nMA3 domain mediates interactions observed between Pdcd4 and eIF4G. Further structural and functional studies of the nMA3 domain of Pdcd4 are required in order to fully understand the contributions of this domain to the inhibition of translation initiation and tumorigenesis by Pdcd4.

Phosphorylation of Pdcd4 by Akt (23) appears to regulate Pdcd4 localization and certain activities. Since the Akt phosphorylation site (Ser457) is not part of the canonical MA3 structure of Pdcd4, it is not surprising that a mutation of this residue that renders it nonphosphorylated (Ser457Ala) also failed to affect competition for eIF4A binding. We have previously shown that mutations that abolish eIF4A binding (Asp414Lys and Asp418Ala) also inactivated translation inhibition by full-length Pdcd4 (29). These results, along with our observation that mutations at the Akt site did not affect translation inhibition by Pdcd4 cMA3, agree with the conclusion that Akt phosphorylation does not influence cMA3 function. Furthermore, we observed that the mutation in the Akt site (S457) in the full-length protein also does not affect Pdcd4 function. Consistent with our observation, a recent report from Dorrello et al. (6) supports our hypothesis that the other Akt site (S67) in the N terminus of the protein may play a significant role in the regulation of Pdcd4 expression and activity. In summary, our analyses indicate that although Akt phosphorylation may be important for posttranslational regulation of Pdcd4, phosphorylation at residue S457 clearly does not influence either binding of eIF4A to the cMA3 domain or the translation inhibition function of Pdcd4.

The translation initiation activity of eIF4A is important for mRNAs containing complex 5′ untranslated regions, many of which are involved in promoting oncogenesis. Given the ability of the cMA3 domain to inhibit this function on its own, this domain might form the basis for the design of drugs that target the translation of a subset of mRNAs to prevent or treat cancer.

ACKNOWLEDGMENTS

We express our gratitude to Zbyszek Dauter for help in analyzing the crystallographic data utilized in this study and to Hsin-Shen Yang and Tobias Schmid for comments and suggestions. Diffraction data were collected at the Southeast Regional Collaborative Access Team beamline 22-ID, located at the Advanced Photon Source, Argonne National Laboratory.

Use of the Advanced Photon Source was supported by the U.S. Department of Energy, Office of Science, Office of Basic Energy Sciences, under contract no. W-31-109-Eng-38. This project was supported by the Intramural Research Program of the NIH, National Cancer Institute, Center for Cancer Research. The research of N.L.-L. and A.N.S. was supported by National Cancer Institute postdoctoral fellowships.

REFERENCES

1. **Baker, N. A., D. Sept, S. Joseph, M. J. Holst, and J. A. McCammon.** 2001. Electrostatics of nanosystems: application to microtubules and the ribosome. Proc. Natl. Acad. Sci. USA **98:**10037–10041.
2. **Bauer, C., N. Brass, I. Diesinger, K. Kayser, F. A. Grasser, and E. Meese.** 2002. Overexpression of the eukaryotic translation initiation factor 4G (eIF4G-1) in squamous cell lung carcinoma. Int. J. Cancer **98:**181–185.
3. **Bellsolell, L., P. F. Cho-Park, F. Poulin, N. Sonenberg, and S. K. Burley.** 2006. Two structurally atypical HEAT domains in the C-terminal portion of human eIF4G support binding to eIF4A and Mnk1. Structure **14:**913–923.
4. **Budihardjo, I., H. Oliver, M. Lutter, X. Luo, and X. Wang.** 1999. Biochemical pathways of caspase activation during apoptosis. Annu. Rev. Cell Dev. Biol. **15:**269–290.
5. **Cmarik, J. L., H. Min, G. Hegamyer, S. Zhan, M. Kulesz-Martin, H. Yoshinaga, S. Matsuhashi, and N. H. Colburn.** 1999. Differentially expressed protein Pdcd4 inhibits tumor promoter-induced neoplastic transformation. Proc. Natl. Acad. Sci. USA **96:**14037–14042.
6. **Dorrello, N. V., A. Peschiaroli, D. Guardavaccaro, N. H. Colburn, N. E. Sherman, and M. Pagano.** 2006. S6K1- and βTRCP-mediated degradation of PDCD4 promotes protein translation and cell growth. Science **314:**467–471.
7. **Emsley, P., and K. Cowtan.** 2004. Coot: model-building tools for molecular graphics. Acta Crystallogr. D **60:**2126–2132.
8. **Goke, A., R. Goke, A. Knolle, H. Trusheim, H. Schmidt, A. Wilmen, R. Carmody, B. Goke, and Y. H. Chen.** 2002. DUG is a novel homologue of translation initiation factor 4G that binds eIF4A. Biochem. Biophys. Res. Commun. **297:**78–82.
9. **Holm, L., and C. Sander.** 1993. Protein structure comparison by alignment of distance matrices. J. Mol. Biol. **233:**123–138.
10. **Jansen, A. P., C. E. Camalier, and N. H. Colburn.** 2005. Epidermal expression of the translation inhibitor programmed cell death 4 suppresses tumorigenesis. Cancer Res. **65:**6034–6041.

11. **Jansen, A. P., C. E. Camalier, C. Stark, and N. H. Colburn.** 2004. Characterization of programmed cell death 4 in multiple human cancers reveals a novel enhancer of drug sensitivity. Mol. Cancer Ther. **3:**103–110.
12. **Kadlec, J., E. Izaurralde, and S. Cusack.** 2004. The structural basis for the interaction between nonsense-mediated mRNA decay factors UPF2 and UPF3. Nat. Struct. Mol. Biol. **11:**330–337.
13. **Korneeva, N. L., E. A. First, C. A. Benoit, and R. E. Rhoads.** 2005. Interaction between the NH2-terminal domain of eIF4A and the central domain of eIF4G modulates RNA-stimulated ATPase activity. J. Biol. Chem. **280:** 1872–1881.
14. **Korneeva, N. L., B. J. Lamphear, F. L. Hennigan, W. C. Merrick, and R. E. Rhoads.** 2001. Characterization of the two eIF4A-binding sites on human eIF4G-1. J. Biol. Chem. **276:**2872–2879.
15. **Lohi, O., A. Poussu, Y. Mao, F. Quiocho, and V. P. Lehto.** 2002. VHS domain—a longshoreman of vesicle lines. FEBS Lett. **513:**19–23.
16. **Marcotrigiano, J., I. B. Lomakin, N. Sonenberg, T. V. Pestova, C. U. Hellen, and S. K. Burley.** 2001. A conserved HEAT domain within eIF4G directs assembly of the translation initiation machinery. Mol. Cell **7:**193–203.
17. **Mazza, C., M. Ohno, A. Segref, I. W. Mattaj, and S. Cusack.** 2001. Crystal structure of the human nuclear cap binding complex. Mol. Cell **8:**383–396.
18. **McRee, D. E.** 1999. XtalView/Xfit—a versatile program for manipulating atomic coordinates and electron density. J. Struct. Biol. **125:**156–165.
19. **Misra, S., B. M. Beach, and J. H. Hurley.** 2000. Structure of the VHS domain of human Tom1 (target of myb 1): insights into interactions with proteins and membranes. Biochemistry **39:**11282–11290.
20. **Morino, S., H. Imataka, Y. V. Svitkin, T. V. Pestova, and N. Sonenberg.** 2000. Eukaryotic translation initiation factor 4E (eIF4E) binding site and the middle one-third of eIF4GI constitute the core domain for cap-dependent translation, and the C-terminal one-third functions as a modulatory region. Mol. Cell. Biol. **20:**468–477.
21. **Murshudov, G. N., A. A. Vagin, and E. J. Dodson.** 1997. Refinement of macromolecular structures by the maximum-likelihood method. Acta Crystallogr. D **53:**240–255.
22. **Oberer, M., A. Marintchev, and G. Wagner.** 2005. Structural basis for the enhancement of eIF4A helicase activity by eIF4G. Genes Dev. **19:**2212–2223.
23. **Palamarchuk, A., A. Efanov, V. Maximov, R. I. Aqeilan, C. M. Croce, and Y. Pekarsky.** 2005. Akt phosphorylates and regulates Pdcd4 tumor suppressor protein. Cancer Res. **65:**11282–11286.
24. **Ponting, C. P.** 2000. Novel eIF4G domain homologues linking mRNA translation with nonsense-mediated mRNA decay. Trends Biochem. Sci. **25:**423–426.
25. **Shibahara, K., M. Asano, Y. Ishida, T. Aoki, T. Koike, and T. Honjo.** 1995. Isolation of a novel mouse gene MA-3 that is induced upon programmed cell death. Gene **166:**297–301.
26. **Terwilliger, T. C.** 2003. SOLVE and RESOLVE: automated structure solution and density modification. Methods Enzymol. **374:**22–37.
27. **Waters, L. C., M. Bohm, V. Veverka, F. W. Muskett, T. A. Frenkiel, G. P. Kelly, A. Prescott, N. S. Dosanjh, K. H. Klempnauer, and M. D. Carr.** 3 March 2006. NMR assignment and secondary structure determination of the C-terminal MA-3 domain of the tumour suppressor protein Pdcd4. J. Biomol. NMR [Epub ahead of print.]
28. **Yang, H. S., M. H. Cho, H. Zakowicz, G. Hegamyer, N. Sonenberg, and N. H. Colburn.** 2004. A novel function of the MA-3 domains in transformation and translation suppressor Pdcd4 is essential for its binding to eukaryotic translation initiation factor 4A. Mol. Cell. Biol. **24:**3894–3906.
29. **Yang, H. S., A. P. Jansen, A. A. Komar, X. Zheng, W. C. Merrick, S. Costes, S. J. Lockett, N. Sonenberg, and N. H. Colburn.** 2003. The transformation suppressor Pdcd4 is a novel eukaryotic translation initiation factor 4A binding protein that inhibits translation. Mol. Cell. Biol. **23:**26–37.
30. **Yang, H. S., A. P. Jansen, R. Nair, K. Shibahara, A. K. Verma, J. L. Cmarik, and N. H. Colburn.** 2001. A novel transformation suppressor, Pdcd4, inhibits AP-1 transactivation but not NF-κB or ODC transactivation. Oncogene **20:**669–676.
31. **Yang, H.-S., C. P. Matthews, T. Clair, Q. Wang, A. R. Baker, C. C. H. Li, T.-H. Tan, and N. H. Colburn.** 2006. Tumorigenesis suppressor Pdcd4 downregulates mitogen-activated protein kinase kinase kinase kinase 1 expression to suppress colon carcinoma cell invasion. Mol. Cell. Biol. **26:**1297–1306.
32. **Zakowicz, H., H. S. Yang, C. Stark, A. Wlodawer, N. LaRonde-LeBlanc, and N. H. Colburn.** 2005. Mutational analysis of the DEAD-box RNA helicase eIF4AII characterizes its interaction with transformation suppressor Pdcd4 and eIF4GI. RNA **11:**261–274.
33. **Zimmer, S. G., A. DeBenedetti, and J. R. Graff.** 2000. Translational control of malignancy: the mRNA cap-binding protein, eIF-4E, as a central regulator of tumor formation, growth, invasion and metastasis. Anticancer Res. **20:**1343–1351.